



Optimisation of 4D printed mortar-mini vascular networks (m-MVNs) for built heritage preservation

C. De Nardi^{a,*}, D. Gardner^a, J. Sweeney^b, A. Akkady^b

^a RESCOM Research Group, School of Engineering, Cardiff University, Queen's Buildings, The Parade, Cardiff CF24 3AA Wales, United Kingdom

^b Engineering, Faculty of Engineering and Digital Technologies, University of Bradford, Bradford BD7 1DP England, United Kingdom

ARTICLE INFO

Keywords:

FDM
Self-healing
Lime-based mortars
Built heritage

ABSTRACT

As climate change increases risks to heritage buildings, enhancing repair methods for historic masonry is essential. This paper presents the design and optimisation process for the manufacturing of a novel self-healing technology—named mortar mini-vascular networks (m-MVNs)—intended for installation in mortar joints during joint repair. m-MVNs are Fused Deposition Modelling (FDM)-printed polymer units with interconnected channels designed to store and protect healing agents. When damage in the mortar joint exceeds a threshold, the m-MVNs rupture, releasing the healing agent to initiate the self-repair process. Engineered within a 4D printing framework, the m-MVNs were optimised through iterative design refinement to protect healing agents, with fracture properties ensuring activation under specific stress conditions. The final m-MVN design, manufactured using adaptive slicing from clear polylactide acid (PLA), achieved the best performance in terms of: i) geometrical regularity, ii) mechanical compatibility with hydraulic lime-based mortars, iii) quasi-isotropy, iv) and water-tightness. This breakthrough paves the way for innovative self-healing solutions in heritage conservation.

1. Introduction

In recent years, additive manufacturing (AM) technologies have revolutionised the way physical objects are made. AM unlocks significant and valuable opportunities, enabling the manufacturing of nonstandard geometrical forms of unprecedented complexity, with minimal waste. The term fused deposition modelling (FDM) was trademarked by Stratasys Inc in 1991 [1] and now is one of the most widely used three-dimensional (3D) printing technologies. FDM is a process during which the filament of thermoplastic material is extruded continuously from a hot nozzle in linear segments that are accumulated to create a shape [2]. 3D-printed objects are usually made from engineering plastics, including polylactic acid (PLA), polyethylene (PE), acrylonitrile butadiene styrene (ABS), polyethylene terephthalate (PET), polystyrene (PS), polycarbonate (PC), polycaprolactone (PCL), polyether ether ketone (PEEK), nylon, and thermoplastic urethane (TPU) [3–5]. Fillers, that vary from metals to plant-based additives, can be added to plastics to improve properties, such as surface texture, mechanical strength and material sustainability whilst reducing cost [6,7].

However, conventional 3D printing produces static objects that retain their properties and shape after fabrication. The emergence of

four-dimensional (4D) printing has introduced a paradigm shift by incorporating stimuli-responsive materials that allow printed objects to transform over time in response to external stimuli such as temperature, moisture, light, or magnetic fields [8,9].

The concept of 4D printing was first introduced by Tibbits in 2013 at the Massachusetts Institute of Technology (MIT), where he described it as an extension of 3D printing that integrates smart materials capable of self-transformation [9]. The “fourth dimension” in 4D printing refers to the dynamic behaviour of printed objects, which undergo shape, property, or functional changes over time [10]. This transformation is typically governed by material properties, structural design, and external triggers such as thermal, pneumatic, or chemical stimuli [11,12].

Key materials used in 4D printing include shape-memory polymers (SMPs), hydrogels, and composites with active fillers. These materials enable the realisation of self-healing, reconfigurable, and adaptive structures [3]. This is achieved through the careful design of geometries, with precisely controlled deposition of layers and through the inclusion of different materials or active fibres [8,11,13]. The primary mechanisms driving these transformations are: i) Shape Memory Effect (SME): materials return to a predetermined shape upon exposure to specific stimuli such as heat or light [14,15] ii) Hygroscopic Expansion: some

* Corresponding author.

E-mail addresses: denardic@cardiff.ac.uk (C. De Nardi), gardnerdr@cardiff.ac.uk (D. Gardner), J.Sweeney@bradford.ac.uk (J. Sweeney), a.akkady2@bradford.ac.uk (A. Akkady).

<https://doi.org/10.1016/j.matdes.2025.114118>

Received 31 March 2025; Received in revised form 24 April 2025; Accepted 18 May 2025

Available online 19 May 2025

0264-1275/© 2025 The Authors. Published by Elsevier Ltd. This is an open access article under the CC BY license (<http://creativecommons.org/licenses/by/4.0/>).

hydrogels and bio-inspired materials swell or contract when exposed to moisture, leading to controlled actuation [16,17]; iii) Multi-Material Printing: the strategic arrangement of different materials allows for controlled anisotropic deformations [18].

4D printing has been widely explored across multiple industries. In biomedical engineering, it has enabled the development of self-expanding stents, drug delivery systems, and tissue scaffolds that adapt to physiological conditions [19]. In aerospace and robotics, deployable structures and morphing wings have been designed to respond to environmental changes [20]. Civil engineering has also benefited, particularly in the development of self-healing materials, such as self-healing concrete and adaptive architectural components [21].

Commonly, time is referred to as the fourth dimension in 4D printing, whereby the transformation of an object over time is considered after being printed [10]. In the current work, this transformation is leveraged to introduce a stimulus-responsive behaviour, enabling self-healing in hydraulic lime-based matrices. Mortar-mini vascular networks (m-MVNs) are FDM-printed units consisting of a system of interconnected channels designed to store and protect healing agents. Units designed for concrete structures (i.e. MVNs) have been studied by the author's previously in [22,23] demonstrating successful outcomes in the recovery of mechanical properties of the concrete structure.

As illustrated in Fig. 1, the healing mechanism relies on the preservation of dormant m-MVNs until a threshold level of damage is reached. At this point, the embedded MVNs within the matrix (e.g., concrete or lime) rupture, releasing the encapsulated healing agent. The fracture properties of m-MVNs are engineered within a 4D printing framework, ensuring a predefined mechanical response that activates healing only under specific stress conditions, thereby extending their effectiveness beyond their shape and capacity to store healing agents. Specifically, these fracture properties are tailored to align with the mechanical characteristics of the host matrix and the application, ensuring that rupture occurs in response to the designed mechanical stresses. These stresses act as external stimuli, triggering the rupture and subsequent controlled release of the healing agent precisely when and where it is needed, thereby enhancing the self-healing efficiency of the system. Table 1 summarises the key aspects that provide the basis for classifying m-MVNs within the 4D printing framework, based on fundamental principles of time-dependent transformation, external stimuli-driven behaviour, functional material change, and engineered design.

Historic masonry structures are integral to cultural identity and heritage. However, they are increasingly at risk due to climate change factors such as rising sea levels, increased precipitation, and extreme weather events. For instance, a report by Historic Environment Scotland indicates that over half of Scotland's historic sites are "at risk" due to such climate-related factors [24]. Increasingly frequent and intense weather events—such as storms, heavy rainfall, and flooding—are accelerating the deterioration of built heritage, particularly in structures composed of porous materials like historic masonry, which are highly susceptible to moisture ingress, salt crystallization, and freeze–thaw cycles [25]. To address the challenges of preserving historic masonry, researchers are exploring self-healing mortars as a sustainable solution. Vucetic et al. [26] studied surface healing in original and replicated medieval mortars from Bač Fortress, Serbia, using a two-component

Table 1

Rationale for the 4D definition of m-MVNs.

| 4D printing principles | Application to MVNs |
|--------------------------------------|--|
| I Time-Dependent Transformation | Mortar-mini vascular networks (m-MVNs) rupture over time in response to mechanical stresses, enabling a delayed self-healing mechanism in the host material. |
| II External Stimuli-Driven Behaviour | The rupture of m-MVNs due to mechanical stress aligns with the concept of a pre-designed response to an external trigger. |
| III Functional Change in Material | The self-healing process activated by m-MVNs contributes to a dynamic change in the host material properties. |
| IV Engineered Design for Application | The fracture behaviour of m-MVNs is tailored to match the mechanical characteristics of the host matrix and application, ensuring a controlled and intentional transformation. |

bacterial system (*Sporosarcina pasteurii* DSM 33 and nutrients). Healing was less effective in the original mortars, likely due to insufficient free calcium ions [27]. Moreover, Recent research has aimed at improving the performance of hydraulic lime-based mortars by integrating smart additives [28] and nanomaterials [29]. Santhanam et al. [30] explored the influence of carboxymethyl cellulose (CMC) and alcofine (AF) on the hydraulic and durability characteristics of natural hydraulic lime mortars, demonstrating enhanced freeze–thaw resistance over extended healing periods.

In parallel with biological and chemical approaches, recent advancements have explored self-healing systems such as mini-vascular networks (MVNs). These networks, inspired by natural vascular systems, are embedded within the mortar matrix to enable the delivery of healing agents directly to damaged areas. Initially developed for use in newly constructed concrete structures, the concept of MVNs has been adapted for application in heritage conservation through a process of technology transfer. To meet the specific constraints of historic masonry walls, the design of the MVNs was revisited, resulting in the development of mortar mini-vascular networks (m-MVNs) that fit entirely within the typical thickness of a mortar joint (~10–15 mm). This adaptation ensures compatibility with traditional masonry while maintaining the capacity for targeted, repeatable self-healing [31]. As illustrated in Fig. 2, if significant sections of masonry have been damaged to the point that mortar joints have lost their function, the so called scucuci technique (i.e. patching) can be used to restore structural continuity while preserving the original blockwork. As part of a new biomimetic approach, the renewed hydraulic lime-based mortar joints incorporate m-MVNs filled with healing agents that are both compatible with the original material and afford the hydraulic lime-based mortar joint the ability to self-heal when damaged.

It is worth noting that this technology is designed to autonomously repair cracks occurring within the mortar joints, while autogenous healing may occur at the interface between the units and the mortar, thereby enhancing adhesion [32].

The aim of the work reported in this paper was to design an m-MVN suitable for masonry restoration and to optimize the 4D printing process to satisfy the requirements for self-healing hydraulic lime-based mortar joints, namely: i) ability to rupture at an appropriate mechanical stress; ii) isotropy along m-MVN ligaments; iii) strong bond properties with

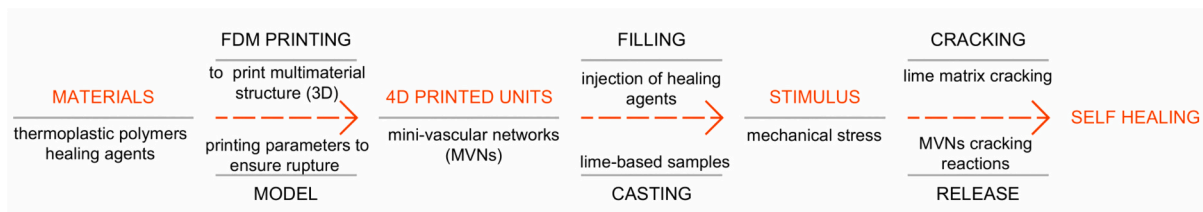


Fig. 1. Summary of mechanisms used for explaining 4D printed mini-vascular networks for self-healing of hydraulic lime-based mortars.

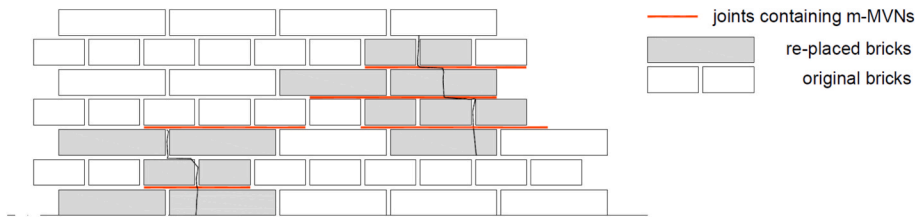


Fig. 2. m-MVNs placement within mortar joints.

lime matrices; and iv) full watertightness when inserted into a hydraulic lime-based matrix.

Section 2 provides details on the materials used in the study and the design description. Section 3 outlines the FDM printing and iteration process to achieve an optimized m-MVN. This includes a detailed description of the four iterations, along with the selected FDM building directions and the support structures used in the printing process. Section 4 presents the methods used to evaluate the performance of each iteration and the rationale for its implementation. Section 5 presents a discussion of the experimental results, analysing each iteration in terms of mechanical behaviour and watertightness efficiency, along with observations of the m-MVNs. The most promising iteration was then embedded in hydraulic lime-based mortar prisms and tested to assess rupture at a serviceable crack width. Conclusion are drawn in Section 6.

2. Materials and design

2.1. Materials

In this study, a commercial clear Polylactic Acid (PLA) supplied by Verbatim with a diameter of 2.85 ± 0.05 mm was used to manufacture the m-MVNs. PLA refers to a class of semi-crystalline degradable polymers, which has been extensively researched and used for FDM [33–35]. It is made from lactic acid derived from fermented plant starch—such as corn [14,36] and has been successfully used for self-healing concrete technologies, including the first generation MVNs [22,37] and connections for continuous networks [38]. During the printing of the samples, the PLA filament was exposed to room temperature. The properties of the PLA polymer [39] are shown in Table 2.

2.2. Mortar-mini-vascular networks (m-MVNs) design

The idea for the m-MVNs came from the need to provide a practical method to supply healing agents in mortar joints with a thickness ranging from 5 to 15 mm. The design meets the need for being directionally invariant, whilst preventing the suction effects associated with closed tubular capsules. The latter is achieved through the multi-ligament design of the m-MVN, which ensures that any crack plane crossing an m-MVN will fracture multiple ligaments thereby avoiding the possibility of negative pressures developing in the liquid healing agent. The protrusions (ribs) on the m-MVN ligaments were designed to anchor the m-MVN to the matrix, thereby limiting the degree of sliding and promoting m-MVN fracture when crossed by a crack. As represented in Fig. 3, the concept design was drawn from the idea to manufacture the unit by turning an extruded tube around a spherical shape, so that the m-MVN unit is almost directionally invariant with respect to its mechanical behaviour.

Two designs were evaluated, differing mainly in the number of ribs

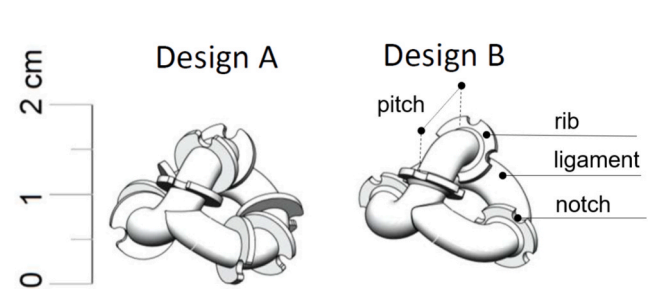


Fig. 3. m-MVNs dimension and design: (A) Ribs with a 6.5 mm pitch and a single notch; (B) Ribs with a 15 mm pitch and four notches per rib.

around the ligaments. Design A featured a 6.5 mm rib to rib spacing (i.e. pitch), while Design B had a 15 mm pitch. To enhance bond properties, Design A incorporated a single 2.2 mm deep notch on each rib, whereas Design B included four notches at 90° intervals around the circumference of each rib. Ultimately, the spherical shape of the m-MVN, coupled with the presence of the ribs, makes the units self-anchor within the host matrix.

2.3. Hydraulic lime-based mortar matrix

The fracture properties of m-MVNs are engineered to be mechanically compatible with hydraulic lime-based mortars—ensuring that rupture occurs under stress conditions corresponding to crack initiation in the host matrix. As cracks form in the mortar due to environmental loading or structural movement, the stress is transferred to the embedded m-MVNs. These are engineered to rupture at stress levels corresponding to those that induce mortar cracking—ensuring that the healing agent is released precisely at the onset of damage, thereby activating the self-healing mechanism. To evaluate the mechanical compatibility of m-MVNs, specifically their rupture at a crack width indicative of in-service cracking (i.e., within the range of 0.05 to 0.1 mm), the m-MVNs were manually positioned in the central third of a 40 mm \times 40 mm \times 160 mm mortar prism mold and secured using 5 mm thick PLA 3D-printed spacers attached to the mold's bottom, as illustrated in Fig. 4. The mortar mix consisted of Natural Hydraulic Lime (NHL) 3.5 (390 kg/m^3), 0–2 mm fine sand (1170 kg/m^3), and water (292 kg/m^3). The moulds were filled in three layers, with the prism specimens initially filled to 5 mm from the base to accommodate one m-MVN before adding more mortar. For seven days after casting, the prisms were kept in the moulds covered with a damp Hessian sheet. After this, samples were placed in laboratory environmental conditions ($20^\circ\text{C} \pm 5^\circ\text{C}$, $\text{RH} \sim 45\%$).

Table 2

Properties of PLA polymer.

| Melting temperature $^\circ\text{C}$ | Glass transition temperature $^\circ\text{C}$ | Nozzle temperature $^\circ\text{C}$ | Heat deflection temperature $^\circ\text{C}$ | Density g/cc | Tensile yield MPa | Tensile elongation % |
|---|--|--|---|-----------------|----------------------|-------------------------|
| 168 | 58 | 200–185 | 49–52 | 1.24 | 63 | 4 |



Fig. 4. m-MVNs position fixed via PLA spacers.

3. Printing and optimisation process

3.1. FDM process

The FDM process was chosen for manufacturing the m-MVNs because it enables the fabrication of complex geometries, allowing for the creation of lightweight, hollow structures while ensuring mechanical integrity and watertightness—critical for the effective encapsulation and controlled release of healing agent. The whole FDM process is illustrated in Fig. 5. It typically comprises six stages; 3D design, tessellation, part orientation and support analyses, slicing and printing.

The CAD design of the m-MVNs was prepared using Solidworks software, converted into STL file format. Mesh editing and correction was performed using Autodesk Meshmixer (Ver 3.5 FREE). An open-source slicer was used to generate G-code from the sample model, i.e. Ultimaker Cura software (free Version: 4.069.04.09.04.11.0), where all the printing parameters were set.

PLA m-MVNs were manufactured using an Ultimaker2+® printer (Utrecht, The Netherlands) with a 0.25 mm diameter nozzle.

3.1.1. STL file generation

3D models are encoded using STL files to represent their surface

geometry. The file format tessellates the surface in unordered triangular patches. This will introduce geometrical error independently from the triangulation refinement. The resolution is governed by two parameters, i.e. maximum chord height and angular tolerance (α), as shown in Fig. 5(b). In order to generate a model that is sufficiently accurate while also maintaining an acceptable file size for loading into Cura, chord deviation and angle tolerance values of 0.13 mm and 2.08 degrees, respectively, were chosen and retained. After importing the STL files into the Meshmixer software, the first step was the model preparation, which includes an automatic repair of any errors in the grid of the meshes that make up a model. The file was then refined by setting the solid accuracy and mesh density to 400 (Fig. 5(b)).

3.1.2. Uniform and adaptive slicing

The process of slicing involves the intersection of the CAD model with a set of horizontal planes to identify specific two-dimensional outlines (contours) which will be later manufactured by material deposition (layers). The parts manufactured through layer deposition show a noticeable step-like effect, as depicted in Fig. 6. This inaccuracy reflects the deviation of the surface of the CAD model and the vertically constructed FDM part.

Inaccuracies arising from the use of planar triangles (meshes) to approximate curved areas and the “staircase effect” both result in irregular geometries and problems with water tightness in the m-MVN ligaments, as can be seen in Fig. 6(a).

Obtaining water tightness is of particular complexity when combined with the need to maintain a thin and constant wall thickness (see Fig. 6 (b-c)) because the layers’ deposition planes in the m-MVNs have varying angles from 0 to 360°.

To mitigate the staircase effect and achieve watertightness, two methods were tried. Firstly, uniform slicing with a fine 0.06 mm layer height was set for the entire m-MVN unit. A 0.06 mm layer height is the smallest compatible with a 0.25 mm diameter nozzle. Secondly, a method called local adaptive slicing was used to optimise build layer thicknesses and meet designed surface deviation tolerances. By setting adaptive layers in Cura, the layer thickness can be adjusted dynamically by decreasing it in critical areas of the object for higher accuracy and increasing it in non-critical areas for faster printing. Here the purpose was to decrease slice thickness in high curvature regions to meet the cusp height requirements. As can be seen in Fig. 7, the cusp vector C describes the maximum deviation between the unit surface and printed object, created by a staircasing effect [40]. The adaptive slicing reduces the layer thickness such that C is maintained below C n-max.

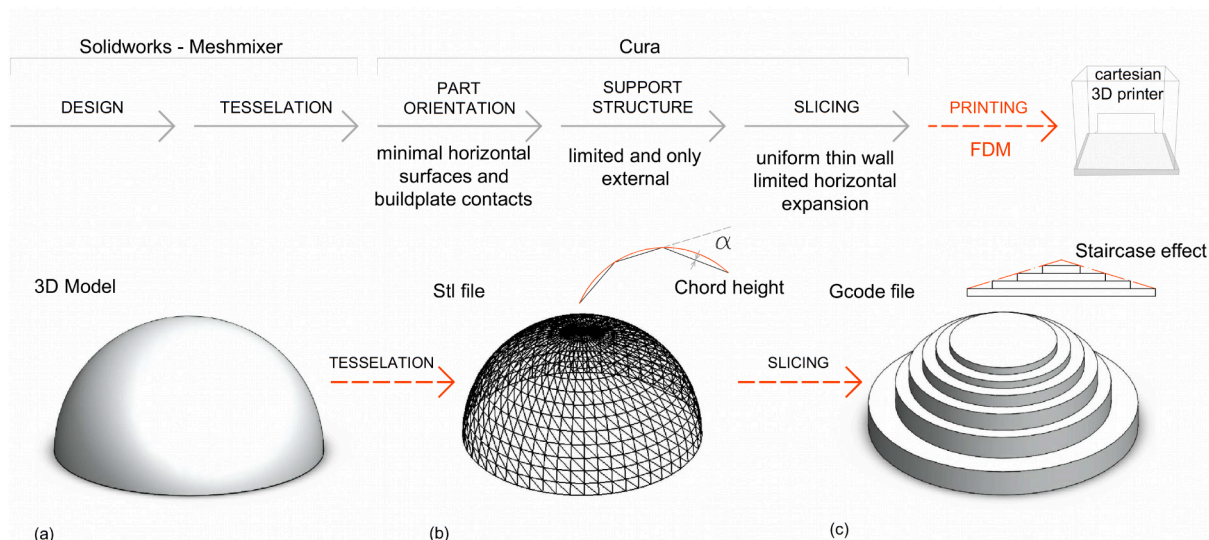


Fig. 5. Steps from 3D model to slicing spheric object for the FDM process.

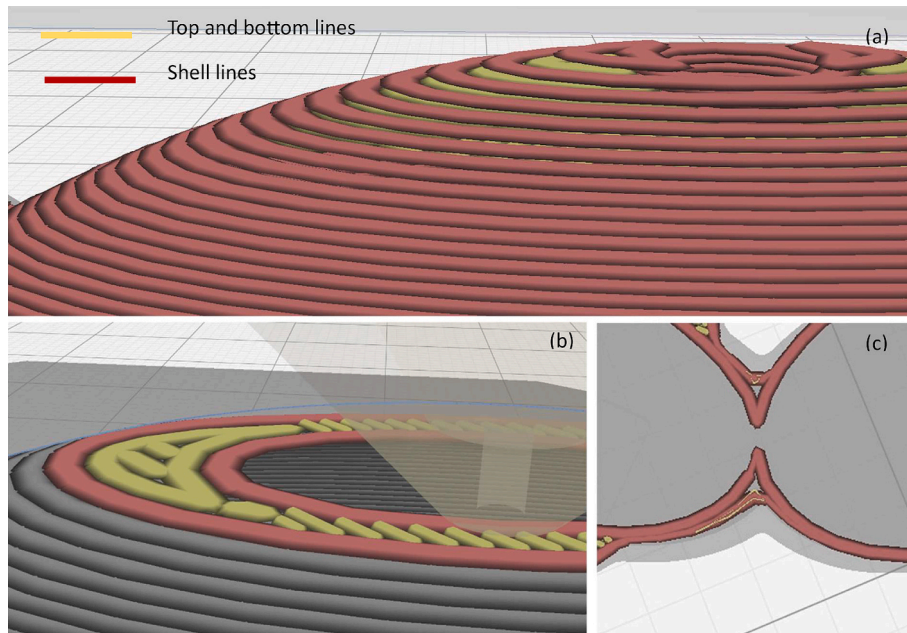


Fig. 6. (a) stair-case effect in m-MVNs, (b) watertightness issues, (c) thin wall issue.

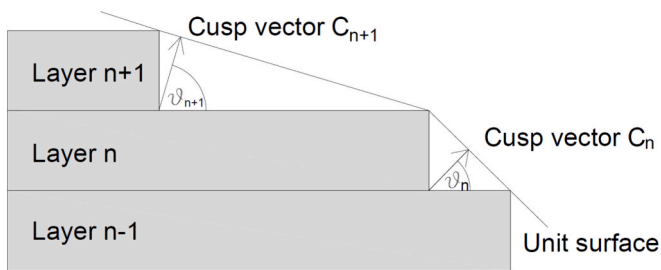


Fig. 7. Cusp height measure, to control the staircase effect.

Design and printing parameters such as wall thickness, density, and infill were adjusted to achieve relatively low strength while meeting all the m-MVNs requirements, including isotropy along ligaments, strong bond properties with lime matrices, and full watertightness when inserted into a hydraulic lime-based matrix.

3.2. Iterations

A total of four iterations were studied with increased improvement: 3D model, parts size, and adjusted printing parameters. Numerous prototypes of each iteration of m-MVN design were produced, with minor modifications to the primary printing parameters to explore the full potential of each iteration

The following sections represent the main characteristics of the most promising prototypes from each iteration. Specific details on their performance, mechanical behaviour and printability can be found in Section 5.

Iteration_I: the initial 3D model in Solidworks, Design A, was drawn as a solid unit, which was hollowed out in the slicing phase. All the printing parameters were derived from previous studies conducted on single channel MVNs [23], including a wall thickness equal to 0.5 mm (0.25 mm x 2 layers) and uniform slicing with 0.06 mm layer height. The layer height was held constant throughout all iterations, except for iteration IV where adaptive slicing was used.

Iteration_II: the main transition to Design B, which remained consistent from that point onwards, featured hollow channels and also included a reduction in the number of ribs per ligament. The ribs both

strengthen the ligaments and disrupt printing continuity, posing challenges in the design. Additionally, to enhance watertightness, the 4 notches per rib were designed with a slightly reduced depth. A small hole was designed to facilitate the injection of healing agent. The wall thickness was reduced to 0.25 mm (0.125 mm x 2 layers).

Iteration_III: the connections between the channels were modified (chamfered) to improve sealing at the joints and facilitate the printing process. Chamfering the edges of the channels creates a smoother transition between them, reducing the likelihood of gaps or irregularities that could compromise the watertightness while also decreasing stress concentrations at the joint interfaces. A wall thickness formed by a single 0.25 mm layer was also considered.

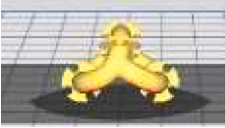
Iteration_IV: to achieve additional improvements in joint quality, connections were further chamfered, while the wall thickness was kept equal to 0.25 mm. Local adaptive slicing was applied, allowing layer heights to vary with a tolerance of 0.02 mm.

In addition, print speed, infill density, and layer height were analysed for their impact on performance, as follows:

- Print speed was reduced to 48 mm/s to improve layer adhesion and precision in small features. Slower speeds helped reduce under-extrusion issues and improved consistency, particularly at junctions between ligaments and ribs—areas critical for watertightness and structural performance.
- Infill density was increased to 100 % in later iterations to ensure the ribs and channels were fully solid where needed. This aimed to reduce internal porosity and prevented leakage of the healing agent.
- Layer height played a central role in balancing detail and speed. A uniform 0.06 mm layer height was used for high resolution in early designs, while adaptive slicing was introduced in Iteration IV to vary layer height based on surface curvature.

The build direction and the use of support structures during printing of MVNs have been previously shown to influence their mechanical and durability performance [22]. As such, three m-MVN orientations were studied with the aim to minimise geometrical irregularities and anisotropies along the channels forming the m-MVNs. These orientations are summarised in Table 3. Additionally, the placement and direction of printing have been designed to minimize the m-MVN's contact with the build plate. This was done with the intention of reducing the risk of

Table 3
Part orientation, top- bottom, support and build plate adhesion parameters.

| Variant | 1 | 2 | 3 |
|------------------------------|---|--|---|
| Orientation |  |  |  |
| | (θ): axis y +105°, axis z +90° | (θ): axis x +90; axis z +90° | (θ): axis z +90° |
| Top/Bottom | | | |
| Bottom layers | 3 | 3 | 5 |
| Initial bottom layers | 5 | 5 | 5 |
| Pattern | Lines | Lines | Concentric |
| Pattern initial layer | Lines | Lines | Concentric |
| Support | | | |
| Support placement | Touching build plate | Touching build plate | Touching build plate |
| Support overhang angle | 50 ° | 50 ° | 50 ° |
| Support pattern | Lines | Lines | Grid |
| Enable support interface | No | No | Yes – 1 mm thickness - concentric pattern |
| Minimum support X/Y distance | 0.25 mm | 0.2 mm | 0.25 mm |
| Minimum support area | 0 mm ² | 1 mm ² | 0 mm ² |

delamination and subsequent weakening of the units during removal from the build plate.

Preliminary testing showed that supports were necessary to improve the geometric accuracy of printed units, regardless of the build direction or attempts to minimize overhangs. Different supports settings and parameters were studied, as described in Table 3. The analysis of the orientations ensured that the supports were only initiated from the build plate, never from the top of the channels or inside of them. The supports were printed using the same filament from which the m-MVN part was made, albeit with a lower printing density.

Among the three options, Variant 3 yielded the most promising results, considering all the required properties. One such property is achieving minimal contact between the brim (a thin, flat border that surrounds the m-MVN unit on the print bed) and the m-MVN unit, preventing delamination of the first layer. Other properties include minimizing the impact of different layer orientations on mechanical

properties, reducing the need for supports, and ensuring easy removal after printing without damaging the units. Subsequently, the orientation depicted in Variant 3 was adopted for all further investigations.

4. Methods

The design iterative process involved geometric modifications, rib reduction, and adjustments to 4D printing parameters, optimizing each iteration based on previous findings. Post-printing evaluation of m-MVNs iterations was threefold. The initial phase involved a visual inspection to identify printing defects, such as gaps between layers, layer shifting or splitting, dimensional accuracy issues, and anisotropies. The second phase involved manually crushing sections of the m-MVNs' ligaments by applying finger pressure to assess their mechanical performance.

Finally, the third phase focused on assessing watertightness. It

involved manually injecting a solution of ink and water into the printed units using a syringe, followed by monitoring for possible leaks over a 24-hour period.

As described in Section 4.1, printed m-MVN iterations underwent tensile testing and analysis to evaluate their mechanical performance. The objective was to explore the boundary values of achievable strength, aiming for the lowest possible strength while maintaining impermeability. This approach ensured that the unit would fail when the hydraulic lime-based mortar matrix failed, while also accounting for the constraints imposed by the 3D printing parameters.

Failures in any of the evaluation phases offer valuable insights by revealing the specific reasons for setbacks and highlighting areas of improvement in the prototype or design. These insights drive subsequent modifications and adjustments in the iterative design and evaluation process, ultimately ensuring that it meets all the required standards and criteria.

After completing all the design optimisation steps, including printability in series and watertightness tests, the best iteration from the trials, filled with dyed liquid, were embedded in lime-mortar prisms and tested in a three-point bend test to evaluate the effective rupture of the unit and determine the crack width at which the rupture and liquid release occur (Section 4.2).

4.1. Testing of m-MVNs

Immediately after printing, three m-MVNs from Iterations I, II, and IV underwent tensile testing, conducted at a constant rate of 50 mm/min until failure, using an Instron 5564 testing machine equipped with a camera a camera to capture videos of the units during testing.

Iteration I was designed to be a stronger and more impermeable unit, featuring a double-wall thickness. In contrast, Iteration II represented the thinnest wall thickness printable with the adopted FDM technology, marking the lower boundary of strength while remaining impermeable. Iteration IV was also tested to assess variations within this range. Iteration III was not subjected to mechanical testing, as it showed only marginal improvements in impermeability compared to the other iterations.

As depicted in Fig. 8, for each type of Iteration, three test configurations were employed to simulate different stresses, allowing variations in strength, failure strain and the mode of failure to be observed. It is worth noting that design A was tested only in configuration 1, as the presence of the intermediate rib made testing in the other configurations impossible.

4.2. Testing compatibility with hydraulic lime-based mortar matrix

A total of six prisms were cast—three containing one m-MVN filled with an aqueous ink solution, and three without. After 28 days, all samples were notched to a depth of 3 mm and tested in flexure using a three-point bend test. The test was conducted under crack mouth opening displacement (CMOD) control at a rate of 0.0001 mm/s, as represented in Fig. 9.

The nominal flexural stress is obtained from the following Equation (1).

$$\sigma^{k_{.28}} = \frac{3Pl}{2bd^2} \tag{1}$$

where P is the peak load, l is the span (120 mm), b is the width of the

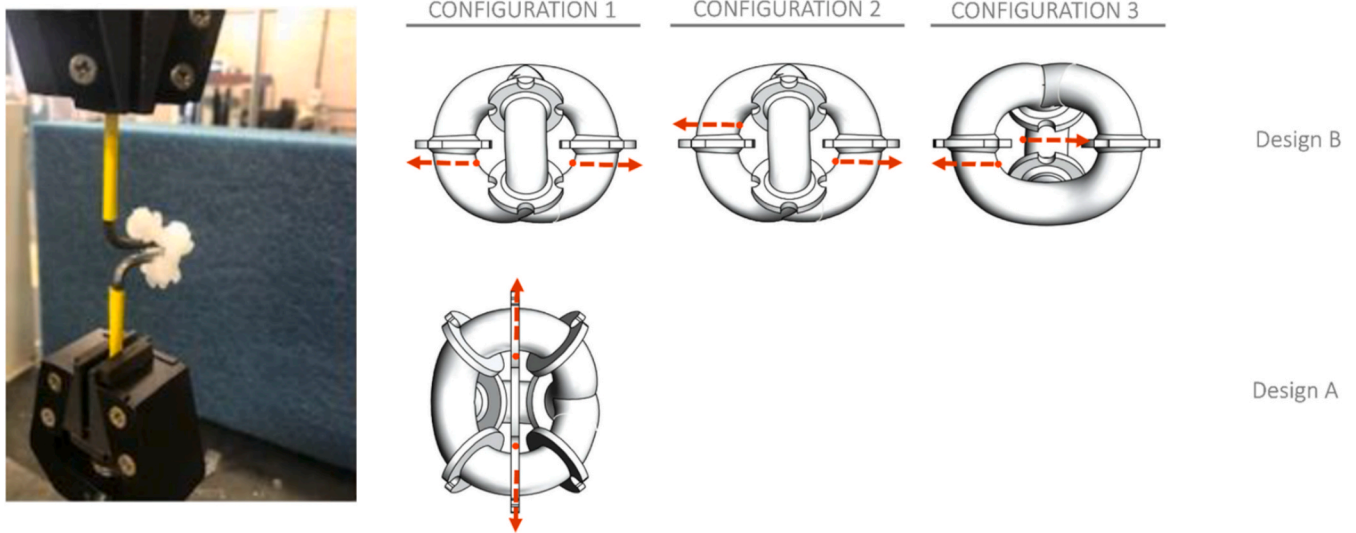


Fig. 8. Tensile test arrangement for model A and B.

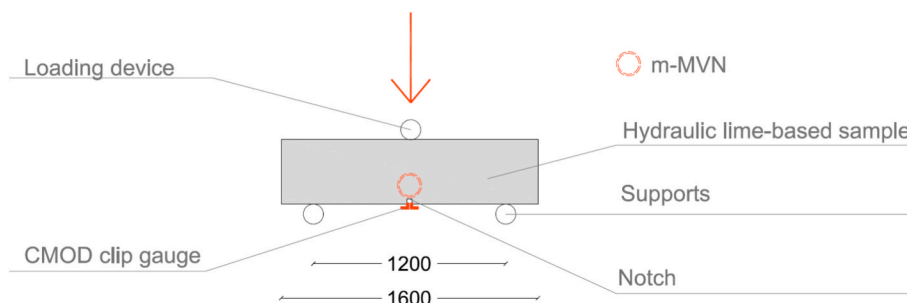


Fig. 9. Flexural test arrangement.

concrete samples (40 mm) and d is the depth (40 mm). Stiffness, defined as the slope of the initial linear portion of the load-CMOD curve was also calculated.

5. Results and discussions

5.1. m-MVN printing

Fig. 10 provides a comprehensive summary of the results, assessments, and test outcomes for all evaluation phases, categorised by the four iterations. Results of tensile tests performed on samples belonging to Iteration I, II and IV are summarised in Tables 4-6, Load vs displacement graphs are presented in Fig. 11.

Iteration_I was printed based on previous MVN printing experiences [22]. As a result of the unit's small size, removing the supports proved to be a challenge: the contact area and the density of the supports themselves meant that their removal often resulted in fractures or irregularities in the ligaments (about 30 % of the time). The process of printing hollow units from a solid model by setting the infill parameters in the slicing phase, resulted in both channels and ribs being hollow. Consequently, ink injected into the unit leaked from the ribs. Iteration I showed the highest tensile force (62.5 N), as the presence of three ribs on each channel (design A) strengthened the m-MVN unit, which is not ideal given the low strength of a lime-mortar matrix.

As a result, Iteration_II was printed from a hollow model with the pitch of the rib being increased to 15 mm (design B) and improved design, i.e. 4 notches per rib were designed with a slightly reduced depth. The wall thickness of the unit was halved compared to Iteration_I. To print solid ribs and uniformly hollow units, the infill was set to 100 %. The print speed was reduced to 48 mm/s in order to improve the accuracy of the overall printing. The main scaffold support parameters were changed and in particular the density was decreased to 5 %.

In Iteration II, several issues arose. Under-extruded layers and uneven walls resulted from extruding a 0.125 mm wall thickness with a 0.25 mm nozzle. This led to irregular geometry, characterised by slight flattening near the base. The printing process was inconsistent, as evidenced by layer misalignment or shifted layers. Significant leakage was also observed from the channels, especially at junctions with the ribs, indicating that the units were not watertight. The change from Design A to Design B, which involved reducing the number of ribs and halving the wall thickness (from 0.5 mm to 0.25 mm), resulted in a tenfold reduction in the force at the first crack, while the displacement at the first crack was halved. However, it became evident that the channels were very fragile and difficult to handle without damage, with 70 % of the units being damaged during the removal of the supports.

For Iteration_III, a few minor changes were made to reduce the inherent fragility of the units and improve junction watertightness. An overlap of 0.0125 mm was used between the layers to create 0.25 mm walls. Concentric infill was used to improve strength homogeneity. In Iteration_III, only a few small holes were evident after the removal of the scaffold supports; generally, surfaces appeared regular and homogeneous. Ribs appeared tight, but occasional minor leaks were observed in the channels, particularly in areas with maximum curvature. Submerging the unit in a thin wax coating resulted in no noticeable deformations due to the wax's heat or the immersion process. However, while the coating initially provided full waterproofing, minor leakage was observed after 24 h.

Consequently, Iteration_IV was printed to reduce the 'staircase effect,' as described above in Section 3.2, by using adaptive slicing. The contact area between the channel and the supports was further reduced.

In Iteration_IV the surfaces remained homogeneous and retained their regular shape even after the removal of scaffold support, a process that occurred successfully without causing any damage in 100 % of the cases. The units were fully watertight, and no leaks were observed after 24 h.

Nevertheless, to safeguard the units against the alkaline environment that arises from their placement within lime matrices, the application of a thin wax coating was deemed a prudent measure for all future m-MVNs. Following the wax coating application, all evaluation phases were repeated, which ultimately led to an optimised m-MVN design.

It is worth noting that m-MVN samples filled with ink (with the injection hole sealed using silicone) and coated with wax were tested by submersion in water, demonstrating full watertight integrity, as confirmed by the absence of ink leakage [31]. Additionally, the filled samples were weighed at regular intervals over a 7-day period, with results showing negligible weight variation, as reported in [41]. Mechanically, the adaptive slicing process resulted in a strength increase of 54 % and 33 % compared to Iteration II in configurations 1 and 3, respectively. However, in configuration 2, Iteration IV was 42 % weaker than Iteration II. Displacements at first crack for Iteration IV were 30 % to 50 % lower than Iteration II in all configurations.

It is important to note that, due to the complex shape of m-MVNs, one ligament must inevitably be printed with an almost horizontal layer, preventing the unit from being fully isotropic. In this context, the adaptive slicing used in Iteration IV seemed beneficial, as the maximum force measured in Configurations 1 and 2 was very close (6.57 N and 7.36 N, respectively).

Fig. 11 shows typical force-displacement results. In Fig. 11(a) for Configuration 1, the higher maximum force and stiffness of Iteration I compared with II and IV is a clear consequence of the greater wall thickness of Iteration I. In this case Iterations I and IV show secondary maxima. This occurs in many instances, when after the first peak, corresponding to the fracture of a ligament, load is transferred to another ligament which then fails; the first failure has the most relevance to in-service performance. In general, the results are highly variable and do not distinguish between Iterations II and IV. Fig. 11(d-g) shows that Iteration IV exhibits an invariant initial fracture position across configurations 1 to 3.

5.2. Lime mortar prisms with embedded m-MVNs

The experimental arrangement is shown in Fig. 12, which depicts a sample containing m-MVNs filled with ink under three-point bend test (a). The results of the flexural tests performed on control samples and samples containing one m-MVN placed in the middle third of the prism are reported in Fig. 13, showing load vs. crack mouth opening displacement (CMOD) responses, and in Table 7.

The flexural strength of prisms with and without m-MVNs (Iteration IV) showed similar results, with values of 0.34 MPa and 0.37 MPa, respectively. A similar trend was observed for the Load-CMOD-based stiffness, where the difference in CoV was only 3 %. Whilst there is a marginal reduction in peak strength, the potential for m-MVNs to provide a post-peak reinforcing effect can be seen in the flexural Load-CMOD responses (Fig. 13). With prudent selection of healing agents there will be further scope to enhance the peak strength and post-peak response of lime mortar materials containing m-MVNs. With regards to breakage of the m-MVN, it was apparent that a CMOD of ~ 0.08 mm was sufficient to rupture the m-MVN ligaments, resulting in ink release, as can be seen in Fig. 13(b). It is important to note that the visibility of the ink at a CMOD of 0.08 mm does not necessarily indicate that this was the point at which the rupture occurred; aqueous ink can easily be

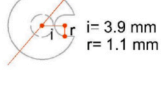
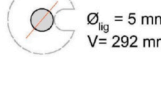
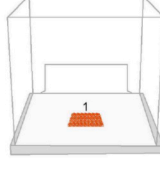
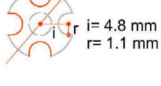
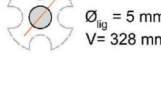
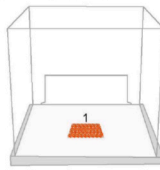
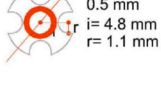
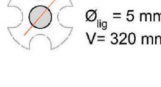
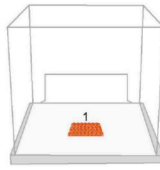
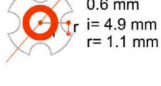
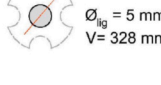
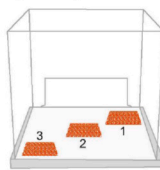
| | 3D MODEL | PARTS SIZE | PRINTING | FUNCTIONALITY | SERIES | |
|---------------|--|---|---|--|--|--|
| ITERATION_I | <p>Design A : solid</p>   | <p>Edge length: 7 mm Ribs: pitch 10 mm Wall thickness: 0.5 mm (0.25x2)</p> <p>$\varnothing_{rib} = 10$ mm</p>  <p>$i = 3.9$ mm $r = 1.1$ mm</p>  <p>$\varnothing_{lig} = 5$ mm $V = 292$ mm³</p> | <p>Filament : clear PLA Printing orientation (ϑ): axis y +105°, axis z +90°</p> <p>Print speed: 60 mm/s</p> <p>Printing temperature: 200 °C</p> <p>Support: Line Density: 10%</p> <p>Brim: length: 250 mm width: 8.0 mm line count: 32</p> | <p>Layer height: 0.06 mm Initial layer height: 0.3 mm</p> <p>Infill line width: 0.25 mm</p> <p>Infill density: 0% Infill pattern: NO</p> | <p>GEOMETRICAL REGULARITY</p> <p>Homogeneous layer deposition: Y</p> <p>Regular geometry: N</p> <p>Impermeability: On ligaments: Y</p> <p>On ribs: N</p> | <p>One at one time</p>  <p>Printing time: 39' Material: 0.14 m</p> |
| ITERATION_II | <p>Design B : hollow</p>   | <p>Edge length: 15 mm Ribs: pitch 15 mm Wall thickness: 0.25 mm (0.125 x2)</p> <p>$\varnothing_{rib} = 10$ mm</p>  <p>$i = 4.8$ mm $r = 1.1$ mm</p>  <p>$\varnothing_{lig} = 5$ mm $V = 328$ mm³</p> | <p>Filament : clear PLA Printing orientation (ϑ): axis z +90°</p> <p>Print speed: 48 mm/s</p> <p>Printing temperature: 200 °C</p> <p>Support: Grid Density: 5%</p> <p>Brim: length: 250 mm width: 8.0 mm line count: 64</p> | <p>Layer height: 0.06 mm Initial layer height: 0.3 mm</p> <p>Infill line width: 0.125 mm</p> <p>Infill density: 100% Infill pattern: Lines</p> | <p>Homogeneous layer deposition: N</p> <p>Regular geometry: N</p> <p>Impermeability: On ligaments: N</p> <p>On ribs: N</p> | <p>One at one time</p>  <p>Printing time: 75' Material: 0.15 m</p> |
| ITERATION_III | <p>Design B : hollow</p>   | <p>Edge length: 15 mm Ribs: pitch 15 mm Wall thickness: 0.25 mm</p> <p>$\varnothing_{rib} = 10$ mm chamfer = 0.5 mm</p>  <p>$i = 4.8$ mm $r = 1.1$ mm</p>  <p>$\varnothing_{lig} = 5$ mm $V = 320$ mm³</p> | <p>Filament : clear PLA Printing orientation (ϑ): axis z +90°</p> <p>Print speed: 60 mm/s</p> <p>Printing temperature: 200 °C</p> <p>Support: Grid Density: 3%</p> <p>Brim: length: 250 mm width: 8.0 mm line count: 32</p> | <p>Layer height: 0.06 mm Initial layer height: 0.3 mm</p> <p>Infill line width: 0.25 mm</p> <p>Infill density: 100% Infill pattern: Concentric</p> | <p>Homogeneous layer deposition: Y</p> <p>Regular geometry: Y</p> <p>Impermeability: On ligaments: N</p> <p>On ribs: N</p> <p>Impermeability after coating with wax: N</p> | <p>One at one time</p>  <p>Printing time: 72' Material: 0.21 m</p> |
| ITERATION_IV | <p>Design B : hollow</p>   | <p>Edge length: 15 mm Ribs: pitch 15 mm Wall thickness: 0.25 mm</p> <p>chamfer = 0.6 mm</p>  <p>$i = 4.9$ mm $r = 1.1$ mm</p>  <p>$\varnothing_{lig} = 5$ mm $V = 328$ mm³</p> | <p>Filament : clear PLA Printing orientation (ϑ): axis z +90°</p> <p>Print speed: 60 mm/s</p> <p>Printing temperature: 185°C</p> <p>Support: Grid Density: 2%</p> <p>Brim: length: 250 mm width: 8.0 mm line count: 32</p> | <p>Layer height: 0.06 mm Initial layer height: 0.25 mm</p> <p>Infill line width: 0.25 mm</p> <p>Infill density: 100% Infill pattern: Concentric</p> <p>Slicing tolerance: Inclusive</p> <p>Adaptive layers: YES Maximum variation: 0.02 mm Variation step size: 0.015 mm</p> | <p>Homogeneous layer deposition: Y</p> <p>Regular geometry: Y</p> <p>Impermeability: On ligaments: Y</p> <p>On ribs: Y</p> <p>Impermeability after coating with wax: Y</p> | <p>One at one time</p> <p>Printing time: 70' Material: 0.19 m</p> <p>Replicability : Y</p>  <p>Series of 3 units Printing time: 211' Material: 0.57m Y</p> |

Fig. 10. Results summary: 3D model, parts size, printing parameters, functionality (Y denotes a positive attribute outcome).

Table 4

Tensile test results with configuration 1.

| Designation | Geometrical parameters mm | | Force at first crackN (CoV%) | Displacement at first crackmm (CoV%) |
|--------------|------------------------------|------------------|---------------------------------|--|
| | Length | Wall thickness | | |
| Iteration I | 13 | 0.5 (0.25 x 2) | 62.5 (9) | 1.44 (18) |
| Iteration II | 13 | 0.25 (0.125 x 2) | 4.27 (10) | 0.84 (16) |
| Iteration IV | 13 | 0.25 (adaptive) | 6.57 (35) | 0.59 (20) |

Table 5

Tensile test results with configuration 2.

| Designation | Geometrical parameters (mm) | | Force at first crackN (CoV%) | Displacement at first crackmm (CoV%) |
|--------------|--------------------------------|------------------|---------------------------------|--|
| | Length | Wall thickness | | |
| Iteration I | 15 | 0.5 (0.25 x 2) | – | – |
| Iteration II | 15 | 0.25 (0.125 x 2) | 12.65 (15) | 1.2 (18) |
| Iteration IV | 15 | 0.25 (adaptive) | 7.36 (10) | 0.66 (31) |

Table 6

Tensile test results with configuration 3.

| Designation | Geometrical parameters (mm) | | Force at first crackN (CoV%) | Displacement at first crackmm (CoV%) |
|--------------|--------------------------------|------------------|---------------------------------|--|
| | Length | Wall thickness | | |
| Iteration I | 5 | 0.5 (0.25 x 2) | – | – |
| Iteration II | 5 | 0.25 (0.125 x 2) | 14.26 (21) | 1.25 (45) |
| Iteration IV | 5 | 0.25 (adaptive) | 18.93 (20) | 0.87 (17) |

absorbed by the matrix and takes time to flow out and become visible from the outside, thus the actual rupture of the m-MVN likely occurred earlier.

5.3. Prospects and limitations

The development of 4D-printed mini-vascular networks (m-MVNs) represents a significant advancement in self-healing hydraulic lime-based mortars for heritage conservation. The iterative optimisation process has demonstrated the feasibility of producing watertight, mechanically responsive units capable of controlled rupture at serviceable crack widths. These findings open new possibilities for integrating smart materials into historical masonry repair, potentially enhancing the durability and resilience of traditional repair methods.

However, several challenges and limitations remain. The current fabrication process relies on FDM printing, which imposes constraints on resolution, repeatability, and large-scale production. Additionally, while the mechanical behaviour of the m-MVNs has been optimised in a controlled laboratory setting, real-world applications may introduce variability due to environmental conditions, material aging, and interactions with different mortar compositions.

Future studies should focus on long-term durability assessments, including the interaction between PLA and the healing agents over extended periods, particularly under alkaline conditions typical of hydraulic lime-based mortars. Investigating the potential for PLA degradation, leaching, or structural weakening due to prolonged exposure to

moisture and chemical reactions is crucial for ensuring sustained performance.

PLA has the advantages of being bio-derived and compostable under controlled conditions. However, in outdoor heritage settings its durability remains uncertain. These units are unlikely to face UV exposure, but they are hydrolytically degradable and will certainly be subjected to moisture and temperature fluctuations. To mitigate degradation, a protective wax coating has already shown promise in shielding the m-MVNs from alkaline moisture exposure. Further research could explore improved coatings or test alternative materials with higher resistance to environmental stresses, while still aligning with conservation principles and sustainability goals.

The flexibility of FDM technologies, combined with the framework established in this study for designing and testing these units, provides a systematic approach that allows for straightforward testing of alternative materials with greater resistance to moisture and alkaline environments.

Healing agents will be analysed with careful consideration of compatibility requirements with both PLA and aerial/hydraulic lime mortars, while also being specifically tailored to counteract distinct forms of degradation. For instance, salt inhibitors could be incorporated to mitigate salt-induced decay, while nanolime dispersions may be employed to enhance consolidation in areas affected by loss of cohesion. Crucially, the proposed system offers the flexibility to be customised at a fine scale, allowing different healing agents to be deployed within the same masonry unit depending on the localised degradation mechanism.

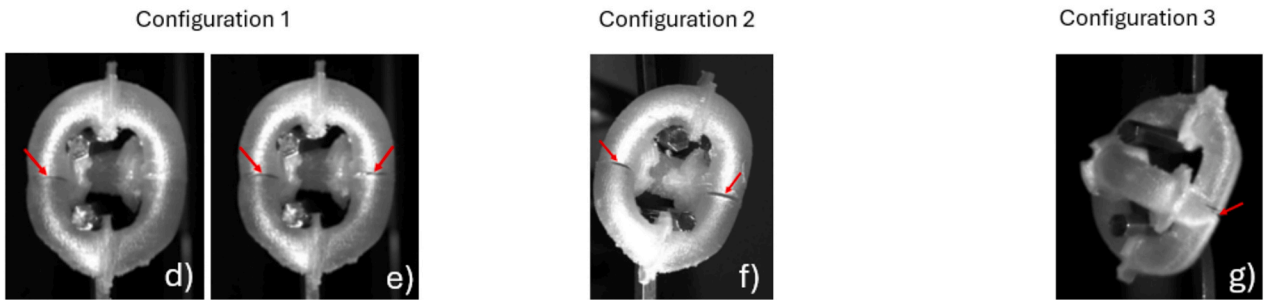
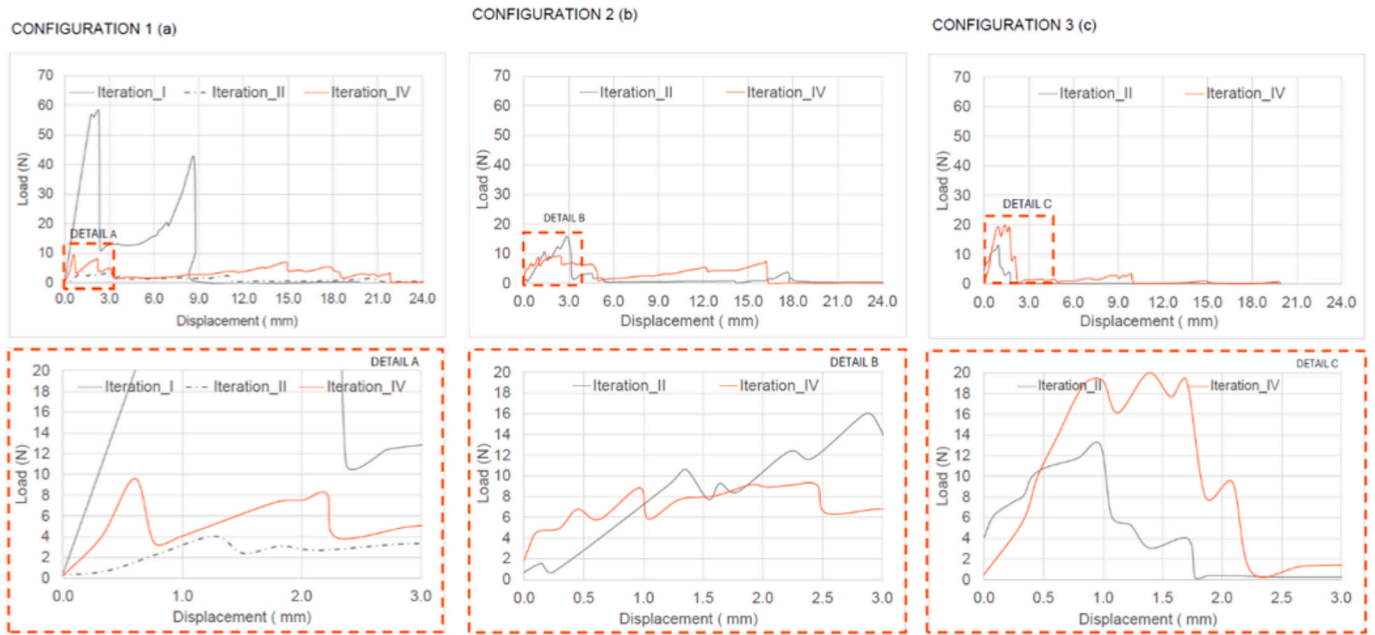


Fig. 11. Tensile tests: configuration 1, iteration I,II,IV (a) configuration 1, iteration I II,IV; (b); configuration 2, iteration II,IV; (c) configuration 3, iteration II, IV. Iteration IV. Configuration 1 typical result (d) Initial fracture at arrowed site. (e) Subsequent frame after time interval of 160 ms showing second fracture. Configuration 2 typical result. (f) Arrows show cracks, appearing on the same frame and so within 20 ms of one another. configuration 3 typical result. Configuration 3, g) Cracking at the arrowed site.

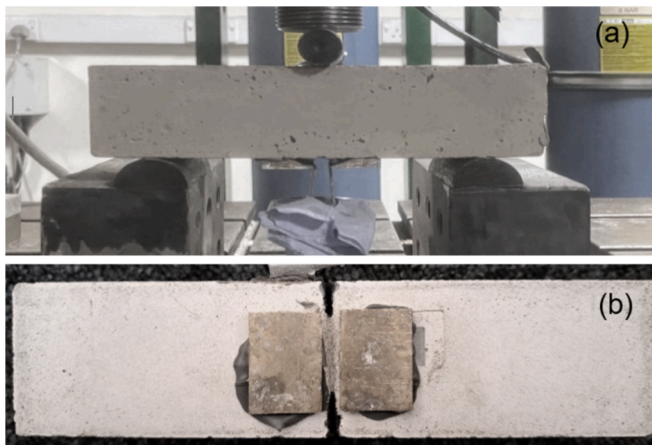


Fig. 12. samples under three-point bend test (a), evidence of m-MVNs rupture at CMOD of ~ 0.08 mm (b).

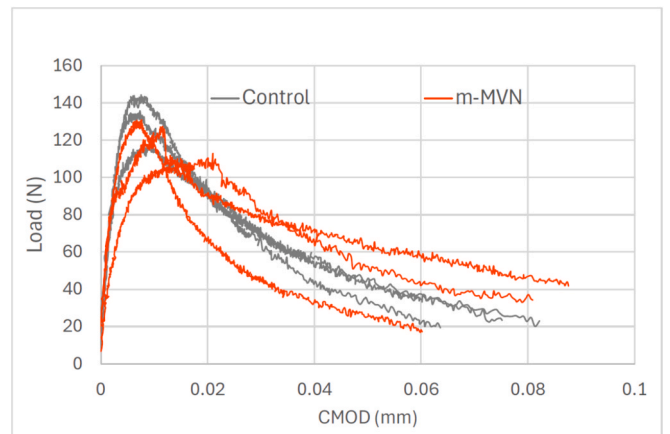


Fig. 13. Flexural load-CMOD response of control samples and samples containing one m-MVN.

Table 7

Flexural strength results of samples with and without m-MVNs tested at 28 days.

| Designation | σ_{k-28} MPa (CoV%) | Stiffness N/mm (CoV%) |
|-------------|----------------------------|-----------------------|
| Control | 0.37 (9) | 28990.6 (13) |
| m-MVN | 0.34 (8) | 27999.0 (21) |

This adaptive approach enables a targeted response to heterogeneous decay phenomena, enhancing the effectiveness and sustainability of the intervention.

6. Conclusion

When significant sections of masonry are damaged to the extent that mortar joints no longer function properly, a technique known as “scuci-cuci” or patching is employed. This method consists of maintaining the structural integrity and preserving the original blocks (i.e., stones or bricks), while applying new mortar to replace the deteriorated material.

This paper proposes the integration of a self-healing technology called mini vascular networks (m-MVNs) into these hydraulic lime-based mortar joints. An innovative m-MVN unit composed of 4D-printed interconnected channels, specifically designed to securely store and safeguard healing agents is herein proposed. The concept involves releasing the stored healing agents when damage exceeds a predefined threshold, triggered by the rupture of the m-MVNs within the mortar matrix, ensuring precise delivery to damaged areas.

Four iterations of m-MVN were studied based on a design concept where the unit is fabricated by wrapping an extruded tube around a spherical shape. Two designs varying in the number of ribs were studied, uniform and adaptive slicing were applied to improve printing results. From the analyses of the results presented in the paper, the following main conclusions have been drawn:

- Key parameters to manufacture accurate units of such a complex design include precise STL file generation with refined and corrected meshing. In order to minimize the m-MVN's contact with the build plate and ensure that the orientation minimizes geometrical irregularities and anisotropies, it was found that orientation of the z-axis at +90°, a grid support pattern, and a brim were the best solutions. Clear PLA was confirmed as an appropriate material for prototyping m-MVN iterations.
- 4 m-MVN iterations were studied with increased improvement in each. Transitioning from a design with fewer ribs per ligament, shallower notches and chamfered channel connections improved the watertightness and ease of printing. Based on these adjustments, using local adaptive slicing with a 0.02 mm tolerance in layer height (Iteration IV) achieved watertightness without significantly increasing the strength
- Among the four iterations, Iteration IV demonstrated the best performance. The average maximum force at the first crack, considering the three tested configurations, is 10.9 N, with a corresponding average displacement of 0.7 mm. While achieving complete isotropy along the ligaments is challenging due to shape complexity, adaptive slicing in Iteration IV had a positive impact on the results.
- Iteration IV, when embedded in natural hydraulic lime prismatic samples, showed good bond between the unit's ligaments and the hydraulic lime-based matrix. Mechanical compatibility has been observed, with no significant changes in flexural strength or stiffness, confirming the suitability of this technology. The visibility of ink at a CMOD of 0.08 mm suggests successful liquid release but does not necessarily mark the exact rupture point.

In summary, 4D printed mini vascular networks (m-MVNs) offer a promising self-healing solution for hydraulic lime-based mortars, effectively storing healing agents without leakage and releasing them

under suitable stress levels. This innovation opens new possibilities for improving the durability and longevity of lime mortar joints used in the restoration of historical masonry. The iterative design optimisation of 4D-printed m-MVNs, particularly in Iteration IV where adaptive slicing was used, achieved significant advancements in performance, including watertightness and effective healing agent storage.

Future research will focus on optimizing healing agent formulations and assessing durability to expand the technology's application in heritage conservation.

CRedit authorship contribution statement

C. De Nardi: Writing – review & editing, Writing – original draft, Visualization, Validation, Supervision, Project administration, Methodology, Investigation, Funding acquisition, Formal analysis, Data curation, Conceptualization. **D. Gardner:** Writing – review & editing, Conceptualization. **J. Sweeney:** Data curation. **A. Akkady:** Data curation.

Declaration of competing interest

The authors declare that they have no known competing financial interests or personal relationships that could have appeared to influence the work reported in this paper.

Acknowledgements

This research was funded by the Leverhulme Trust ECF2022-235. The authors would also like to acknowledge the considerable help and expertise of PAP.

Data availability

Data will be made available on request.

References

- [1] Stratasys, “FDM Trademark of Stratasys, Inc. - Registration Number 1663961 - Serial Number 74133656.” Accessed: Feb. 11, 2023. [Online]. Available: <https://trademarks.justia.com/741/33/fdm-74133656.html>.
- [2] S.H. Masood, in: *Advances in Fused Deposition Modeling*, Elsevier, 2014, <https://doi.org/10.1016/B978-0-08-096532-1.01002-5>.
- [3] C.M. González-Henríquez, M.A. Sarabia-Vallejos, J. Rodríguez-Hernandez, Polymers for additive manufacturing and 4D-printing: materials, methodologies, and biomedical applications, *Prog. Polym. Sci.* 94 (2019) 57–116, <https://doi.org/10.1016/j.progpolymsci.2019.03.001>.
- [4] V. Mazzanti, L. Malagutti, F. Mollica, FDM 3D printing of polymers containing natural fillers: a review of their mechanical properties, *Polymers (Basel)* 11 (7) (2019), <https://doi.org/10.3390/polym11071094>.
- [5] S.C. Ligon, R. Liska, J. Stampfl, M. Gurr, R. Mühlhaupt, Polymers for 3D printing and customized additive manufacturing, *Chem. Rev.* 117 (15) (2017) 10212–10290, <https://doi.org/10.1021/acs.chemrev.7b00074>.
- [6] S. Bhagia, et al., Critical review of FDM 3D printing of PLA biocomposites filled with biomass resources, characterization, biodegradability, upcycling and opportunities for biorefineries, *Appl. Mater. Today* 24 (2021), <https://doi.org/10.1016/j.apmt.2021.101078>.
- [7] J.S. Borah, D.S. Kim, Recent development in thermoplastic/wood composites and nanocomposites: a review, *Korean J. Chem. Eng.* 33 (11) (2016) 3035–3049, <https://doi.org/10.1007/s11814-016-0183-6>.
- [8] F. Momeni, S.M. Mehdi Hassani, N.X. Liu, J. Ni, A review of 4D printing, *Mater. Des.* 122 (2017) 42–79, <https://doi.org/10.1016/j.matdes.2017.02.068>.
- [9] S. Tibbits, “The emergence of ‘4D printing,’” TED Conference. Accessed: Feb. 11, 2023. [Online]. Available: https://www.ted.com/talks/skylar_tibbits_the_emergence_of_4d_printing.
- [10] Y.S. Lui, W.T. Sow, L.P. Tan, Y. Wu, Y. Lai, H. Li, 4D printing and stimuli-responsive materials in biomedical aspects, *Acta Biomater.* 92 (2019) 19–36, <https://doi.org/10.1016/j.actbio.2019.05.005>.
- [11] D. Saritha, D. Boyina, A concise review on 4D printing technology, *Mater. Today Proc.* 46 (2021) 692–695, <https://doi.org/10.1016/j.matpr.2020.12.016>.
- [12] M. Bodaghi, R. Noroozi, A. Zolfagharian, M. Fotouhi, S. Norouzi, 4D printing self-morphing structures, *Materials* 12 (8) (2019), <https://doi.org/10.3390/ma12081353>.
- [13] M. Bodaghi, R. Noroozi, A. Zolfagharian, M. Fotouhi, S. Norouzi, 4D printing self-morphing structures, *Materials* 12 (8) (2019), <https://doi.org/10.3390/ma12081353>.

- [14] T. Maharana, S. Pattanaik, A. Routaray, N. Nath, A.K. Sutar, Synthesis and characterization of poly(lactic acid) based graft copolymers, *React. Funct. Polym.* 93 (2015) 47–67, <https://doi.org/10.1016/j.reactfunctpolym.2015.05.006>.
- [15] L. Bonetti, D. Natali, S. Pandini, M. Messori, M. Toselli, G. Scalet, 4D printing of semi-crystalline crosslinked polymer networks with two-way shape-memory effect, *Mater. Des.* 238 (2024) 112725, <https://doi.org/10.1016/j.matdes.2024.112725>.
- [16] A. Le Duigou, V. Keryvin, J. Beaugrand, M. Pernes, F. Scarpa, M. Castro, Humidity responsive actuation of bioinspired hygromorph biocomposites (HBC) for adaptive structures, *Compos. A Appl. Sci. Manuf.* 116 (2019) 36–45, <https://doi.org/10.1016/j.compositesa.2018.10.018>.
- [17] A. Le Duigou, T. Fruleux, R. Matsuzaki, G. Chabaud, M. Ueda, M. Castro, 4D printing of continuous flax-fibre based shape-changing hygromorph biocomposites: towards sustainable metamaterials, *Mater. Des.* 211 (2021) 110158, <https://doi.org/10.1016/j.matdes.2021.110158>.
- [18] K. Benyahia, et al., Design for multi-material 4D printing: development of an algorithm for interlocking blocks assembly generation, *Procedia CIRP* 119 (2023) 396–401, <https://doi.org/10.1016/j.procir.2023.02.144>.
- [19] M. Ramezani, Z. Mohd Ripin, “4D Printing in Biomedical Engineering: Advancements, Challenges, and Future Directions,” Jul. 01, 2023, *Multidisciplinary Digital Publishing Institute (MDPI)*. doi: 10.3390/jfb14070347.
- [20] K. Ntounoglou, P. Stavropoulos, D. Mourtzis, “4D printing prospects for the aerospace industry: A critical review,” in *Procedia Manufacturing*, Elsevier B.V., 2018, pp. 120–129. doi: 10.1016/j.promfg.2018.11.016.
- [21] A.A. Firoozi, A.A. Firoozi, A systematic review of the role of 4D printing in sustainable civil engineering solutions, *Heliyon* 9 (10) (2023) e20982, <https://doi.org/10.1016/j.heliyon.2023.e20982>.
- [22] C. De Nardi, D. Gardner, D. Cristofori, L. Ronchin, A. Vavasori, T. Jefferson, Advanced 3D printed mini-vascular network for self-healing concrete, *Mater. Des.* 230 (2023) 111939, <https://doi.org/10.1016/j.matdes.2023.111939>.
- [23] C. De Nardi, D. Gardner, A.D. Jefferson, Development of 3D printed networks in self-healing concrete, *Materials* 13 (6) (2020) 1328, <https://doi.org/10.3390/ma13061328>.
- [24] G. Houston, V. Glindmeier, C. Hermann, “Adapting historic places to climate change Proceedings of the international virtual conference of the project Adapt Northern Heritage Acknowledgements Editors.” [Online]. Available: <http://nationalarchives.gov.uk/doc/opengovernment-licence/version/3/www.adaptnorthernheritage.org>.
- [25] M. Mosoarca, A.I. Keller, C. Petrus, A. Racolta, Failure analysis of historical buildings due to climate change, *Eng. Fail. Anal.* 82 (2017) 666–680, <https://doi.org/10.1016/j.engfailanal.2017.06.013>.
- [26] S. Vucetic, et al., Functional mortars for conservation of cultural heritage structures, *IOP Conf. Ser. Mater. Sci. Eng.* 949 (1) (2020), <https://doi.org/10.1088/1757-899X/949/1/012091>.
- [27] S. Vučić, et al., Bio-stimulated surface healing of historical and compatible conservation mortars, *Materials* 16 (2) (2023), <https://doi.org/10.3390/ma16020642>.
- [28] C. De Nardi, S. Bullo, L. Ferrara, L. Ronchin, A. Vavasori, Effectiveness of crystalline admixtures and lime/cement coated granules in engineered self-healing capacity of lime mortars, *Mater. Struct./Materiaux et Constructions* 50 (4) (2017), <https://doi.org/10.1617/s11527-017-1053-3>.
- [29] D. Ergenç, A. Sierra-Fernandez, M.del M. Barbero-Barrera, L.S. Gomez-Villalba, R. Fort, Assessment on the performances of air lime-ceramic mortars with nano-Ca(OH)₂ and nano-SiO₂ additions, *Constr. Build. Mater.* 232 (2020) 117163, <https://doi.org/10.1016/j.conbuildmat.2019.117163>.
- [30] K. Santhanam, R. Ramadoss, Sustainability development and performance evaluation of natural hydraulic lime mortar for restoration, *Environ. Sci. Pollut. Res.* 29 (52) (2022) 79634–79648, <https://doi.org/10.1007/s11356-022-21019-x>.
- [31] C. De Nardi, R. Giorgi, Mortar-mini-vascular networks filled with nanolimes: an innovative biomimetic approach for enhancing resilience in built heritage, *Constr. Build. Mater.* 472 (2025) 140881, <https://doi.org/10.1016/j.conbuildmat.2025.140881>.
- [32] C. De Nardi, C. Brito de Carvalho Bello, L. Ferrara, A. Cecchi, “Self-healing lime mortars: overview of an experimental investigation from material to subassembly scale,” in *International Conference on Sustainable Materials, Systems and Structures (SMSS 2019) Durability, monitoring and repair of structures*, 2019, pp. 652–659.
- [33] S.M.D. Tezerjani, M.S. Yazdi, M.H. Hosseinzadeh, The effect of 3D printing parameters on the shape memory properties of 4D printed polylactic acid circular disks: an experimental investigation and parameters optimization, *Mater. Today Commun.* 33 (2022) 104262, <https://doi.org/10.1016/j.mtcomm.2022.104262>.
- [34] A. Milovanović, et al., Influence of printing parameters on the eligibility of plane-strain fracture toughness results for PLA polymer, *Procedia Struct. Integrity* 41 (2022) 290–297, <https://doi.org/10.1016/j.prostr.2022.05.034>.
- [35] A. Milovanović, et al., Comparative analysis of printing parameters effect on mechanical properties of natural PLA and advanced PLA-X material, *Procedia Struct. Integrity* 28 (2020) 1963–1968, <https://doi.org/10.1016/j.prostr.2020.11.019>.
- [36] T. Maharana, B. Mohanty, Y.S. Negi, Melt–solid polycondensation of lactic acid and its biodegradability, *Prog. Polym. Sci.* 34 (1) (2009) 99–124, <https://doi.org/10.1016/j.progpolymsci.2008.10.001>.
- [37] C. De Nardi, D. Gardner, A. Jefferson, T. Selvarajoo, G. Evans, The Development of Mini-Vascular Networks for Self-Healing Concrete, in: *In Durable Concrete for Infrastructure under Severe Conditions Durable Concrete for Infrastructure under Severe Conditions*, 2019, pp. 19–23.
- [38] D. Robert, J. Tony, G. Diane, Development and testing of vascular networks for self-healing cementitious materials, *J. Mater. Civ. Eng.* 33 (7) (2021) 04021164, [https://doi.org/10.1061/\(ASCE\)MT.1943-5533.0003802](https://doi.org/10.1061/(ASCE)MT.1943-5533.0003802).
- [39] VERBATIM, “PLA Verbatim properties.” Accessed: Feb. 11, 2023. [Online]. Available: <https://www.verbatim-europe.co.uk/en/prod/verbatim-pla-filament-2-85mm-1kg-natural-transparent-55326/>.
- [40] A. Dolenc, I. Mäkelä, Slicing procedures for layered manufacturing techniques, *Comput. Aided Des.* 26 (2) (1994) 119–126, [https://doi.org/10.1016/0010-4485\(94\)90032-9](https://doi.org/10.1016/0010-4485(94)90032-9).
- [41] C. De Nardi, D. Gardner, T. Jefferson, Biomimicry in Built heritage: Mini Vascular Networks for Self-healing Lime-based Mortars, in: *In SUBLime Conference 2024 towards the next Generation of Sustainable Masonry Systems: Mortars, Renders, Plasters and Other Challenges*, 2024, pp. 152–153.